Applied Catalysis B: Environmental 304 (2022) 120954

Contents lists available at ScienceDirect

Applied Catalysis B: Environmental

journal homepage: www.elsevier.com/locate/apcatb

A synergetic strategy to construct anti-reflective and anti-corrosive Co-P/WS_x/Si photocathode for durable hydrogen evolution in alkaline condition

Sijie Li [a,b], Huiwen Lin [b,*], Gaoliang Yang [a,b], Xiaohui Ren [a,b], Shunqin Luo [a,b], Xu-sheng Wang [b,d], Zhi Chang [c], Jinhua Ye [a,b,e,**]

[a] Graduate School of Chemical Sciences and Engineering, Hokkaido University, Sapporo 060-0814, Japan
[b] International Center for Materials Nanoarchitectonics (WPI-MANA), National Institute for Materials Science (NIMS), 1-1 Namiki, Tsukuba, Ibaraki 305-0044, Japan
[c] Energy Technology Research Institute, National Institute of Advanced Industrial Science and Technology (AIST), 1-1-1, Umezono, Tsukuba 305-8568, Japan
[d] School of Materials Science and Engineering, Zhejiang Sci-Tech University, Hangzhou 310018, China
[e] TJU-NIMS International Collaboration Laboratory, School of Material Science and Engineering, Tianjin University, Tianjin 300072, PR China

ARTICLE INFO

Keywords:
Planar p-Si photocathode
Anti-corrosive WS_x protective layer
Anti-reflective Co-P cocatalyst
Alkaline media
Photoelectrochemical hydrogen evolution

ABSTRACT

Developing durable Si-based photoelectrochemical hydrogen evolution reaction in alkaline media is attracting attention in device-level water splitting, but still faces a trade-off between the alkalic corrosion resistance and light transmission for Si photocathodes. Herein, a synergetic strategy is proposed to employ an anti-reflective Co-P film cocatalyst modulated via self-assembly of protective-layer WS_x onto Si photocathode. The controllable WS_x thin-film efficiently ensures the excellent anti-alkali corrosion of Si semiconductors, and serves as an appropriate nucleation base to modulate the structure of Co-P cocatalyst to possess anti-reflection. The optimal Co-P/WS_x/Si photocathode exhibits an onset potential of + 0.47 V vs. reversible hydrogen electrode (V_{RHE}), a photocurrent density of − 25.1 mA cm^{-2} at 0 V_{RHE}, and superior durability of up to 300 h at 0 V_{RHE} in 1.0 M KOH electrolyte. These findings offer a facile and effective approach for the further development of durable Si-based photoelectrochemical devices.

1. Introduction

Photoelectrochemical (PEC) water splitting is a promising method to convert solar energy into renewable hydrogen fuel. It involves two half-reactions of hydrogen evolution (HER) at the photocathode and oxygen evolution (OER) at the photoanode, which are generally carried out in highly acidic and alkaline solutions, respectively. As the OER shows more sluggish kinetics to require higher overpotential in acid solutions than HER in an unseparated compartment, conducting HER in alkaline solutions will be preferable with OER [1–4].

While alkaline solutions result in severe corrosion on Si, the most widely studied photocathode in acidic electrolytes for PEC HER [5–8], a protection layer is usually utilized to separate the Si photocathode from alkaline solutions. For instance, TiO_2 has proven to be a good protection layer for Si photocathodes via atomic layer deposition [9,10]. However, these Si photocathodes with dense TiO_2 protection layers need to be combined with precious metal cocatalysts to counter the limitation of light transmission [9–12]. Therefore, designing an appropriate thickness of the protection layer is critical to achieving good alkali resistance, facile electron transfer, and efficient light transmittance to Si. Transition metal chalcogenide such as WS_2 and MoS_2 is one of the potential alternatives, benefiting from their ability in atomic layer fabrication and high stability in acid or alkaline solutions [13–15]. Notably, most of the fabrication processes show complexity and are not cost-effective.

On the other hand, decorating effective cocatalysts with less light-blocking is also significant to PEC HER in alkaline solutions. Recently, non-noble metal Co-P cocatalysts have attracted significant attention due to their remarkable catalytic properties along with outstanding stability in alkaline HER [16–19]. Specific examples are CoP [18, 20–25], Co_2P [26,27], Co-P alloys [28], and their derivatives [29–31]. There are also numerous reports on the application of Co-P cocatalysts in PEC HER, but most are under acidic conditions [22–27]. In the mentioned regard, it is highly desirable to fabricate Co-P cocatalysts on Si photocathodes used in alkaline solutions. However, a similar concern

* Corresponding author.
** Corresponding author at: International Center for Materials Nanoarchitectonics (WPI-MANA), National Institute for Materials Science (NIMS), 1-1 Namiki, Tsukuba, Ibaraki 305-0044, Japan.
E-mail addresses: lin.huiwen@nims.go.jp (H. Lin), Jinhua.YE@nims.go.jp (J. Ye).

https://doi.org/10.1016/j.apcatb.2021.120954
Received 14 July 2021; Received in revised form 26 October 2021; Accepted 17 November 2021
Available online 21 November 2021

on the thickness of the protection layer also raises to the Co-P cocatalyst due to their intrinsic light-blocking. Thus, less thickness of Co-P cocatalyst with high efficiency for PEC HER is demand for Si photocathodes. Loading the thin-film Co-P cocatalyst via the electrodeposition is a promising method since its morphology and thickness can be modulated by controlling the electrochemical potential or current and affected by the photocathode interphase, including the protection layer [22,32].

Herein, a WS_x-protected planar p-Si photocathode with anti-reflective Co-P film cocatalyst (denoted as Co-P/WS_x/Si) is designed and proposed for efficient and durable PEC HER in the alkaline electrolyte (1.0 M KOH). This strategy introduces the self-assembled WS_x thin film on the Si surface as a uniform protection layer with moderate charge-transfer conductivity. Meanwhile, the controllable WS_x serve as nucleation sites to modulate and obtain anti-reflective Co-P cocatalyst by photo-assist electrodeposition, forming a robust and complementary architecture. This synergetic integration of Co-P/WS_x/Si photocathode exhibits outstanding PEC HER performances, including an onset potential of 0.47 V_{RHE} and a high photocurrent density of − 25.1 mA cm^{-2} at 0 V_{RHE} under an AM 1.5 G simulated solar illumination. More surprisingly, the Co-P/WS_x/Si photocathode shows superior durability of 300 h at 0 V_{RHE} without visible degradation. This systematic work may pave a new path for planar Si-based PEC-HER applications in alkaline media.

2. Experiment section

2.1. Fabrication of photocathodes

Firstly, the H-terminated p-Si substrates were prepared and adapted from previous literature [13]. As-prepared H-terminated p-Si wafers were immersed in 5/20/30 mM $(NH_4)_2WS_4$-containing 0.5% HF aqueous solutions to prepare 5WS_x/Si, 20WS_x/Si, and 30WS_x/Si, respectively. The Co-P/WS_x/Si photocathode was obtained by the photo-assisted electrodeposition of Co-P catalysts on H-terminated p-Si, 5WS_x/Si, 20WS_x/Si, and 30WS_x/Si substrates. More detailed information is provided in supporting information.

2.2. Characterization of photocathodes

X-ray film diffraction and X-ray photoelectron spectroscopy (XPS, VG-ESCA Mark II) with monochromatized Al Kα radiation were used to determine the crystal structures and surface valence states. Atomic force microscopy (AFM, Nano Navi II), scanning electron microscopy (SEM, JSM-6701F), and transmission electron microscope (TEM, JEM-2100F) were applied to analyze the morphologies of as-obtained samples. Ultraviolet-visible (UV–vis) absorption spectra were measured utilizing a spectrophotometer (UV-2600, Shimadzu, Japan). The charge carrier transfer and separation of target samples were investigated by photoluminescence (PL) emission (FP-6500).

2.3. PEC measurements

The PEC measurements were carried out on an electrochemical workstation (ALS/CH model 660D) using a three-electrode cell system in 1.0 M KOH at AM 1.5 G solar simulation (100 mW·cm^{-2}), which contained a graphite rod as the counter electrode and a Hg/HgO (1.0 M NaOH) electrode as the reference electrode. The exposure area of the photocathode is 0.4 cm^2. Linear sweep voltammograms (LSV) were obtained. Mott–Schottky curves were performed from − 0.4 to + 0.6 V_{RHE} at 1000 Hz. The onset potential (V_{on}) is defined as the potential that derives a photocurrent density of − 0.1 mA cm^{-2}. Electrochemical impedance spectroscopy (EIS) tests were obtained at various conditions (0.01–100 000 Hz). All the potentials could be transformed to the RHE using the equation: $E_{RHE} = E - IR + 0.059 \times pH + E_{Hg/HgO}$, where E is the experimental potential, $E_{Hg/HgO}$ is equal to + 0.12 V_{RHE}, the pH of 1.0 M KOH is measured to be around 13.6, I and R are the photocurrent density (mA·cm^{-2}) and the internal resistance (Ω) of electrolyte contact, respectively.

3. Results and discussion

3.1. Synthesis and characterization of WSx protective layers

The self-assembly procedure of thin-film WS_x as a protective layer on H-terminated p-Si is schematically illustrated in Fig. 1a. Specifically, the thin-film WS_x is obtained through H-terminated p-Si immersed in WS_4^{2-}-containing HF aqueous solutions, which is adapted from our previous study.[13] As shown in atomic force microscopy (AFM) images, the bare H-terminated p-Si has an atomically smooth surface (Fig. 1b). After the H-terminated p-Si immersed in HF aqueous solutions with increasing concentrations of WS_4^{2-}, the average thicknesses of WS_x thin-film increased to approximately 3 nm (Fig. 1c–e), which is displayed intuitively in 3D images (Fig. S1, Supporting information). The thin-film WS_x is not dense and even enough on p-Si using the 5 mM WS_4^{2-} reactant (5WS_x/Si), while its uniformity is significantly improved when the WS_4^{2-} concentration increases to 20 mM (20WS_x/Si). Increasing the concentration to 30 mM (30WS_x/Si) results in excessive growth of WS_x nanoparticles. These preliminary results show that a moderate 20 mM WS_4^{2-} reactant could ensure a uniform WSx protective layer formation.

X-ray photoelectron spectroscopy (XPS) is applied to determine the valence states and chemical composition of WS_x/Si photocathodes. The survey spectra (Fig. S2) confirm the W, S, O, and Si elements. In Fig. 1f for the high-resolution S 2p spectra, two peaks at 151.1 and 168.3 eV correspond to Si 2s and Si 2s plasmon are observed [33]. Additional peaks appear at around 163 eV, assigned to S 2p. It can be deconvolved into two doublets of S $2p_{3/2}$ and S $2p_{1/2}$. To be specific, the lower binding energy doublets at 162.3 eV (S $2p_{3/2}$) and 163.0 eV (S $2p_{1/2}$) are attributed to the S element of the 2 H phase, and the higher binding energy doublets at 163.4 eV (S $2p_{3/2}$) and 164.4 eV (S $2p_{1/2}$) could be assigned to disordered S atoms in the unsaturated S^{2-} in WS_x. Among the studied WS_x/Si, 20WS_x/Si shows a much higher intensity of S 2p peaks than 5WS_x/Si. While when the WS_4^{2-} concentration continues to increase to 30 mM, no noticeable intensity change is observed. In Fig. 1g for W 4f spectra, the dominant peaks at 33.2 and 35.5 eV are assigned to W $4f_{7/2}$ and W $4f_{5/2}$, respectively. An additional peak of approximately 38.5 eV is assigned to high valence states of W^{VI}, indicating the partially oxidized WS_x due to the air exposure of its surface and uncomplete reduction reaction of WS_4^{2-} [34]. The intensity change of W 4f shows a similar tendency as that of S 2p peaks when the WS_4^{2-} concentration increases.

Combining the AFM and XPS analyses, it is proved that the thin-film WS_x reaches a saturated and uniform morphology from 20 mM WS_4^{2-} solution onward. That of lower than 20 mM will make the thin-film WS_x uneven on the Si surface, which might show an insufficient protective role in alkaline solutions. To confirm the protective role of the thin-film WS_x for Si in alkaline solutions, the as-prepared WS_x/Si wafers were soaked in 1.0 M KOH solution for 12 h. Compared with the scanning electron microscopy (SEM) image of the smooth surface of original bare Si (Fig. S3), the SEM image in Fig. S4a shows that the bare Si surface is severely etched with deep pits larger than 1.0 μm^2 after immersing in 1.0 M KOH solution. The etched pits are significantly reduced in WS_x/Si (Fig. S4b–d), among which 20WS_x/Si and 30WS_x/Si already exhibit outstanding alkalic resistance with few slight scratches.

3.2. Characterization of Co-P/WSx/Si photocathodes

The Co-P cocatalysts were then deposited on WS_x/Si via photo-assisted electrodeposition. Without thin-film WS_x on Si, the morphology of Co-P cocatalyst on Si (Co-P/Si) presents dispersed particles with a diameter of approximately 200 nm (Fig. 2a). A large area of Si surface is exposed between the Co-P particles in Co-P/Si (the inset of Fig. 2a). While with thin-film WS_x on Si, the morphology and size of Co-P

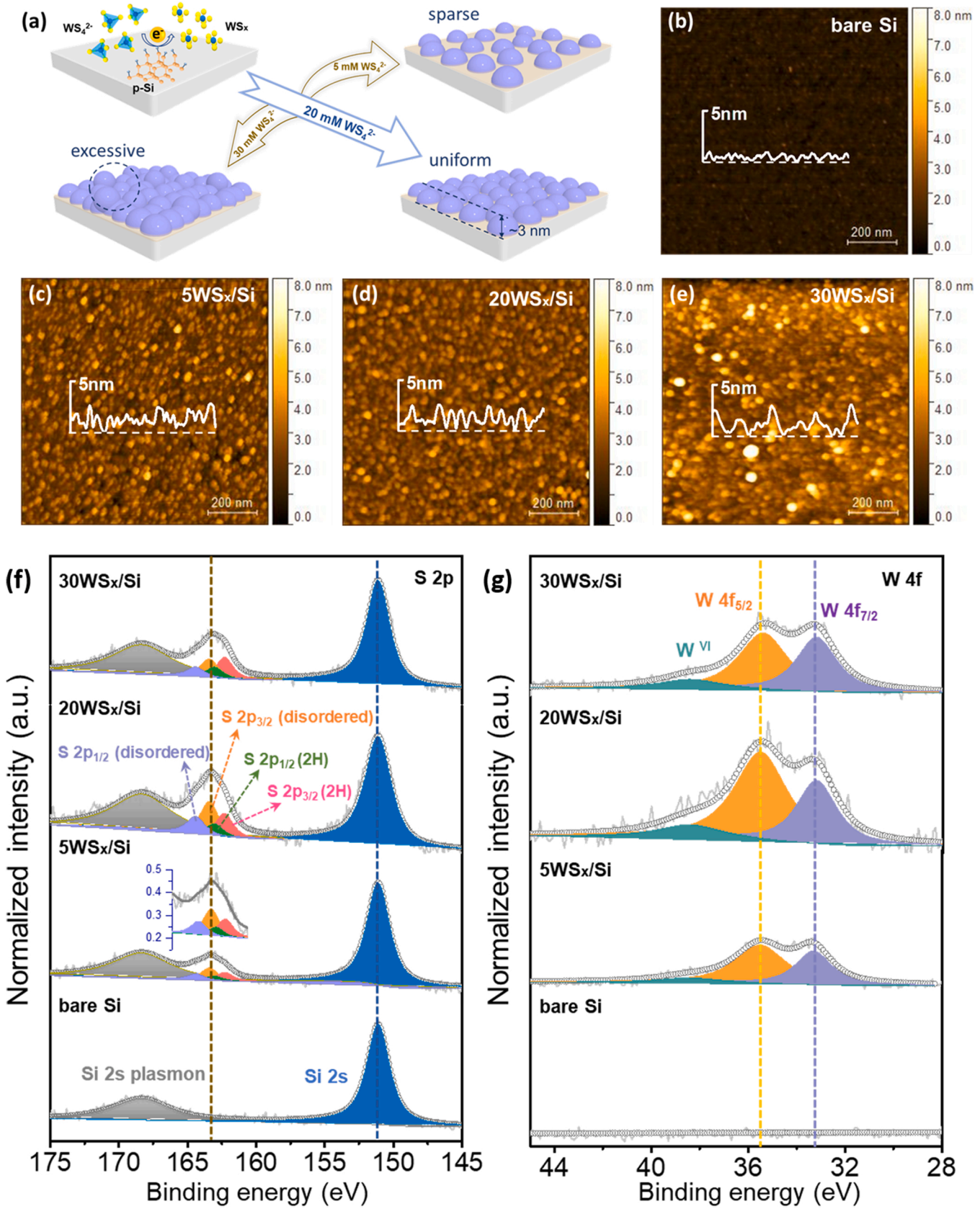

Fig. 1. (a) Schematic illustration for self-assembled deposition of WS_x on p-Si. AFM images of (b) bare Si, (c) $5WS_x$/Si, (d) $20WS_x$/Si, and (e) $30WS_x$/Si. The height profiles along the corresponding dashed lines are shown as the inset Figures. High-resolution XPS spectra of (f) S 2p and (g) W 4f for bare Si, $5WS_x$/Si, $20WS_x$/Si, and $30WS_x$/Si. All the spectra are normalized by the intensity of Si 2s as the reference.

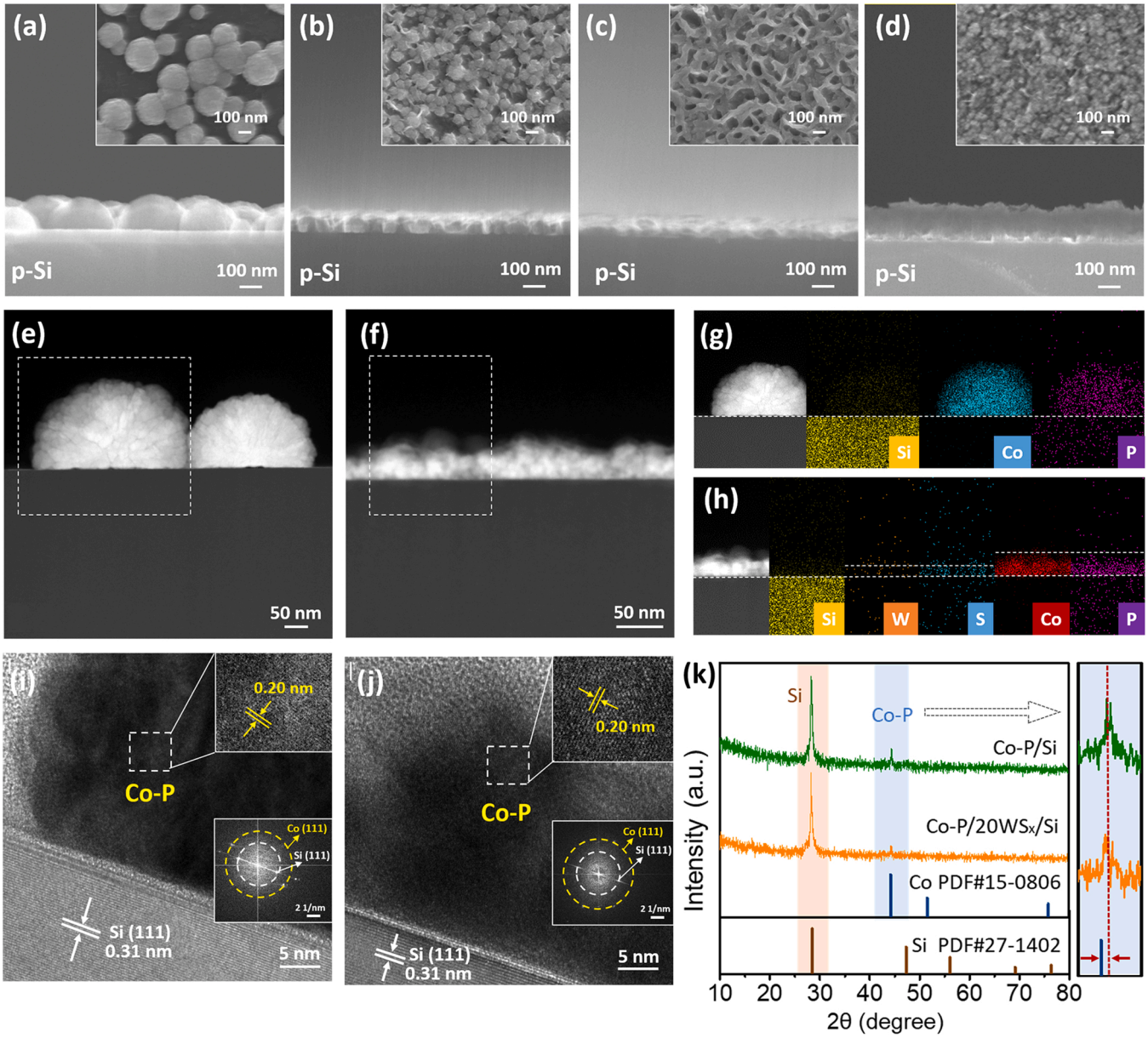

Fig. 2. SEM images of (a) Co-P/Si, (b) Co-P/5WS_x/Si, (c) Co-P/20WS_x/Si, and (d) Co-P/30WS_x/Si. (e–f) HAADF-STEM images, (g–h) EDS mapping images, (i–j) HR-TEM images, and the corresponding SAED images inset of Co-P/Si and Co-P/20WS_x/Si, respectively. (k) The thin-film XRD patterns of Co-P/Si and Co-P/20WS_x/Si.

cocatalysts change accordingly. The Co-P particles (Fig. 2b) deposited on the 5WS_x/Si (Co-P/5WS_x/Si) have smaller sizes and a more compact distribution than the Co-P/Si. In Co-P/20WS_x/Si (Fig. 2c), a Co-P film about 50 nm thick is formed, evenly covering the photocathode surface. It is worth noting that, in the inset of Fig. 2c, the porous Co-P surface can provide a large specific surface area and more active sites, which is conducive to full contact with the electrolyte during the PEC-HER process. However, the Co-P film in Co-P/30WS_x/Si becomes much thicker and denser than the other two Co-P/WS_x/Si (Fig. 2d). Such a thick Co-P cocatalyst layer is likely to block the light absorption of Si semiconductors. Through the above analysis, along with AFM and SEM observations, it is found that the thin-film WS_x in Co-P/20WS_x/Si could be not only efficient in protecting Si from alkaline solution but also a suitable nucleation base to obtain uniform Co-P film with moderate thickness.

The high-angle annular dark-field scanning transmission electron microscopy (HAADF-STEM) images in Fig. 2e and f further confirm the difference in the morphologies of Co-P cocatalysts within Co-P/Si and Co-P/20WS_x/Si. The energy-dispersive spectroscopy (EDS) mapping was carried out to analyze the element distribution therein. The elements of Co, P, and Si in Co-P/Si (Fig. 2g) are uniformly distributed, corresponding to a bilayer structure of cocatalyst/semiconductor. For Co-P/20WS_x/Si, in addition to the uniform distribution of Co, P, and Si elements, the W and S elements in WS_x present between Co-P and Si, forming a trilayer structure of cocatalyst/protector/semiconductor. Therefore, it is confirmed that the WS_x thin film has an impact on the subsequent Co-P deposition. The unsaturated S in the thin-film WS_x is considered to have an attractive force to concentrate the Co^{2+} ions near the interphase in the electrodepositing solutions. Thus, it leads to more Co-P nuclei formation, finally resulting in uniform Co-P cocatalyst with smaller size in Co-P/20WS_x/Si.

X-ray diffraction (XRD) is conducted to analyze the compositions of Co-P cocatalysts within Co-P/20WS_x/Si and Co-P/Si, as shown in Fig. 2k. The characteristic peak at 28.4° is indexed to the (111) facet of Si (JCPDS no. 27-1402), and the peak of Co-P shifts to a slightly higher angle at 44.4° compared with the (111) facet of Co at 44.2° (JCPDS no.

15-0806), as shown in the enlarged image of Fig. 2k. This phenomenon is in good accordance with previous literature about Co-P alloy made by electrodeposition method [35–37], because the relatively low content of P with smaller atomic radius in as-deposited Co-P has such an effect on Co. The P content in Co-P cocatalyst is estimated to be about 22% from the relative XPS peak area and corresponding Relative Sensitivity Factors (The detailed calculation steps in the Experimental Section of Supporting information), which almost corresponds to the atomic ratio of Co and P elements in the EDS result (Table S1, listed in Supporting information). The high-resolution transmission electron microscopy (HR-TEM) images of Co-P/Si and Co-P/20WS_x/Si are further shown in Fig. 2i–j. The interplanar space of 0.31 nm corresponds to the (111) direction of Si, and the d-space of 0.20 nm about as-deposited Co-P is associated with the (111) direction of Co, which is obtained by measuring the average of 10 layers. The selected area electron diffraction (SAED) patterns (the inset of Fig. 2i, j) also reveal the corresponding diffraction rings from the inner of Si to the outer of Co. The d-space value of Co-P is a little bit smaller than that of standard Co (111), which is consistent with the influence of a small amount of P on Co-P alloy in the above XRD analysis.

3.3. PEC-HER performances and mechanism analysis

The PEC-HER performances of bare Si, 20WS_x/Si, Co-P/Si, Co-P/5WS_x/Si, Co-P/20WS_x/Si, and Co-P/30WS_x/Si photocathodes were evaluated in 1.0 M KOH solution at a scan rate of 50 mV/s for comparison. Notably, the linear sweep voltammetry (LSV) curves show that the currents for all photocathodes under dark are negligible (dashed line in Fig. 3a). Under light irradiation, the bare Si photocathode shows an onset potential of approximately − 0.04 V_{RHE} in Fig. 3a. Compared with the bare Si, Co-P/Si and Co-P/WS_x/Si photocathodes exhibit positive shifts on the onset potential. Significantly, the Co-P/20WS_x/Si exhibits the optimal onset potential at + 0.47 V_{RHE} among the Co-P/WS_x/Si photocathodes, as summarized in Fig. 3b. It confirms that the Co-P cocatalysts integrating with WS_x can further improve the PEC-HER activity under the alkaline condition, compared with only Co-P cocatalyst. The significantly enhanced PEC-HER performance of Co-P/20WS_x/Si photocathode in the alkaline solution is comparable to the reported Si-based photocathodes (Table S2). It must be noted that the combination of planar Si and non-noble metal cocatalysts in this study is cost-effective. Mott-Schottky measurements were employed to examine why the integration of Co-P cocatalyst with thin-film WS_x can significantly improve the PEC-HER performance. As shown in Fig. 3c, the flat-band potential (the intersection of tangent and x-axis) of the Co-P/20WS_x/Si (+ 0.25 V_{RHE}) is higher than those of the Co-P/Si (+ 0.02 V_{RHE}), 20WS_x/Si (− 0.14 V_{RHE}), and bare Si (− 0.27 V_{RHE}), which corresponds precisely to the positive shifting trend of their onset potentials as analyzed above.

Moreover, the photocurrent densities at 0 V_{RHE} of the studied Co-P/Si and Co-P/WS_x/Si photocathodes are also visually compared in Fig. 3b. The Co-P/Si photocathode without a WS_x protective layer has a much lower photocurrent density (− 10.4 mA cm^{-2}) at 0 V_{RHE} than those of all Co-P/WS_x/Si photocathodes. By contrast, Co-P/20WS_x/Si processes the highest photocurrent density of − 25.1 mA cm^{-2} at 0 V_{RHE}, followed by Co-P/30WS_x/Si with − 23.8 mA cm^{-2}, and Co-P/5WS_x/Si with − 22.8 mA cm^{-2}. Note that the saturated photocurrent densities of as-prepared photocathodes are affected by their optical behaviors. Therefore, Fig. 3d compares the UV–vis reflection spectra of bare Si, 20WS_x/Si, Co-P/Si, and Co-P/5WS_x/Si. The 20WS_x/Si presents only slightly higher reflectance than that of bare Si, which indicates the uniform WS_x thin film prepared from 20 mM WS_4^{2-} has a little optical impact on the light absorption of the Si semiconductor. However, the light reflectance of Co-P/Si is higher than that of bare Si, resulting in a lower saturation photocurrent density (the photocurrent at −0.6 V_{RHE}), which confirms the light-blocking properties of large-size Co-P particles. Actually, the high light reflection of Co-P/Si is the predictable result, well matching with the large gap between the Co-P particles in the above SEM image (Fig. 2a) and visible reflected color observed in the optical picture of Co-P/Si, but none in other Co-P/WS_x/Si samples (Fig. S5). Notably, the optical reflectance result of Co-P/20WS_x/Si in the low-wavelength region is obviously lower than that of bare Si. This result suggests that the Co-P film acts as an anti-reflective cocatalyst in the Co-P/20WS_x/Si photocathode, which may be due to the porous structure of the Co-P film affecting the refractive index, as previously reported [38]. The light

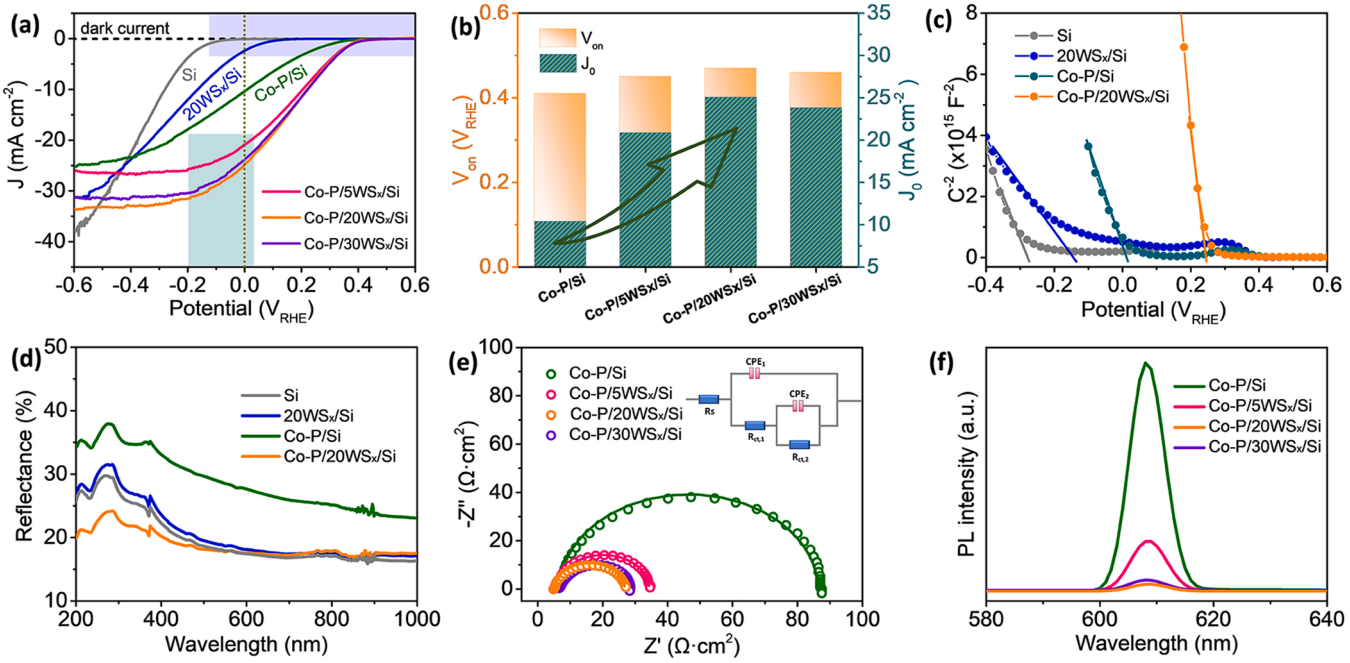

Fig. 3. (a) LSV curves under light, (b) comparison of onset potentials (V_{on}) and photocurrent densities at 0 V_{RHE} (J_0) of bare Si, 20WS_x/Si, Co-P/Si, Co-P/5WS_x/Si, Co-P/20WS_x/Si, and Co-P/30WS_x/Si. (c) Mott-Schottky plots under dark and (d) UV–vis spectra of bare Si, 20WS_x/Si, Co-P/Si, and Co-P/20WS_x/Si. (e) Nyquist plots and fitting figures (solid lines), and (f) PL spectra with an excitation wavelength of 405 nm of Co-P/Si, Co-P/5WS_x/Si, Co-P/20WS_x/Si, and Co-P/30WS_x/Si.

reflection spectra of three Co-P/WS_x/Si are further displayed in Fig. S6. The Co-P/20WS_x/Si gives a lower reflectance in the low-wavelength region than those of Co-P/5WS_x/Si and Co-P/30WS_x/Si, probably because both granular Co-P cocatalyst within Co-P/5WS_x/Si and thicker Co-P cocatalyst within Co-P/30WS_x/Si will hinder light penetration to the underneath Si semiconductor. Such a result reveals that the WS_x thin film has a regulating effect on the morphology and thickness of subsequently deposited Co-P cocatalyst, and ultimately affects the light utilization efficiency of Si-based photocathodes.

The electrochemical impedance spectroscopy (EIS) and photoluminescence (PL) emission are potent tools to evaluate the behavior of charge carrier transfer and separation in Si semiconductors. The EIS measurements of three Co-P/WS_x/Si and Co-P/Si photocathodes were carried out at + 0.40 V_{RHE} under illumination to evaluate the interfacial charge-transfer resistance, as shown in Figs. 3e and S7. Nyquist plots of these photocathodes could be fitted into two semicircles using an equivalent circuit model (inset of Fig. 3e), and the fitting results are presented with solid lines. The equivalent circuit contains a series of resistances (Rs), two constant phase elements consisting of capacitances of the Si substrate (CPE_1) and cocatalyst (CPE_2), and two charge-transfer resistances (R_{ct1} and R_{ct2}). The first semicircle in the high-frequency region reflects the charge-transfer resistance at the interface between Si and cocatalyst (R_{ct1}), and the second arc in the low-frequency region represents another one at the interface of cocatalyst/electrolyte (R_{ct2}), corresponding to the catalytic kinetics [39,40]. The fitted values of R_s, R_{ct1}, and R_{ct2} are listed in Table S3. To be precise, the R_s values of as-prepared photocathodes are almost the same, suggesting the similar resistivity of the electrolyte between working and reference electrodes for these photocathodes. Moreover, all photocathodes exhibit small and similar R_{ct1} values, indicating their good conductivity due to the incorporation of cocatalysts. Next, three Co-P/WS_x/Si photocathodes exhibit much lower R_{ct2} values than that of the Co-P/Si photocathode, which indicates that the Co-P cocatalyst on the thin-film WS_x can efficiently reduce the charge-transfer resistance at the cocatalyst/electrolyte interface. In particular, the lowest R_{ct2} value of Co-P/20WS_x/Si suggests that the thin-film 20WS_x with uniform distribution helps to generate a suitable Co-P cocatalyst to promote electron transfer from Co-P cocatalyst to the electrolyte, thus confirming the improved PEC-HER activities. In addition, PL emission was also carried out to help to judge the behavior of the charge carrier transfer. As shown in Fig. 3f, all Co-P/WS_x/Si and Co-P/Si samples show PL peaks at 608 nm, ascribed to the recombination of photogenerated electron-hole pairs in Si [10]. The Co-P/Si without WS_x thin-film shows the highest PL intensity, while three Co-P/WS_x/Si all show less PL intensity. Specifically, a distinct fluorescence quenching occurs in Co-P/20WS_x/Si, suggesting that the charge carrier recombination is suppressed to the greatest extent. It exemplifies that the more robust compatibility of the Co-P cocatalyst and the thin-film WS_x could efficiently promote the charge transfer, consistent with the EIS analysis and PEC-HER performance.

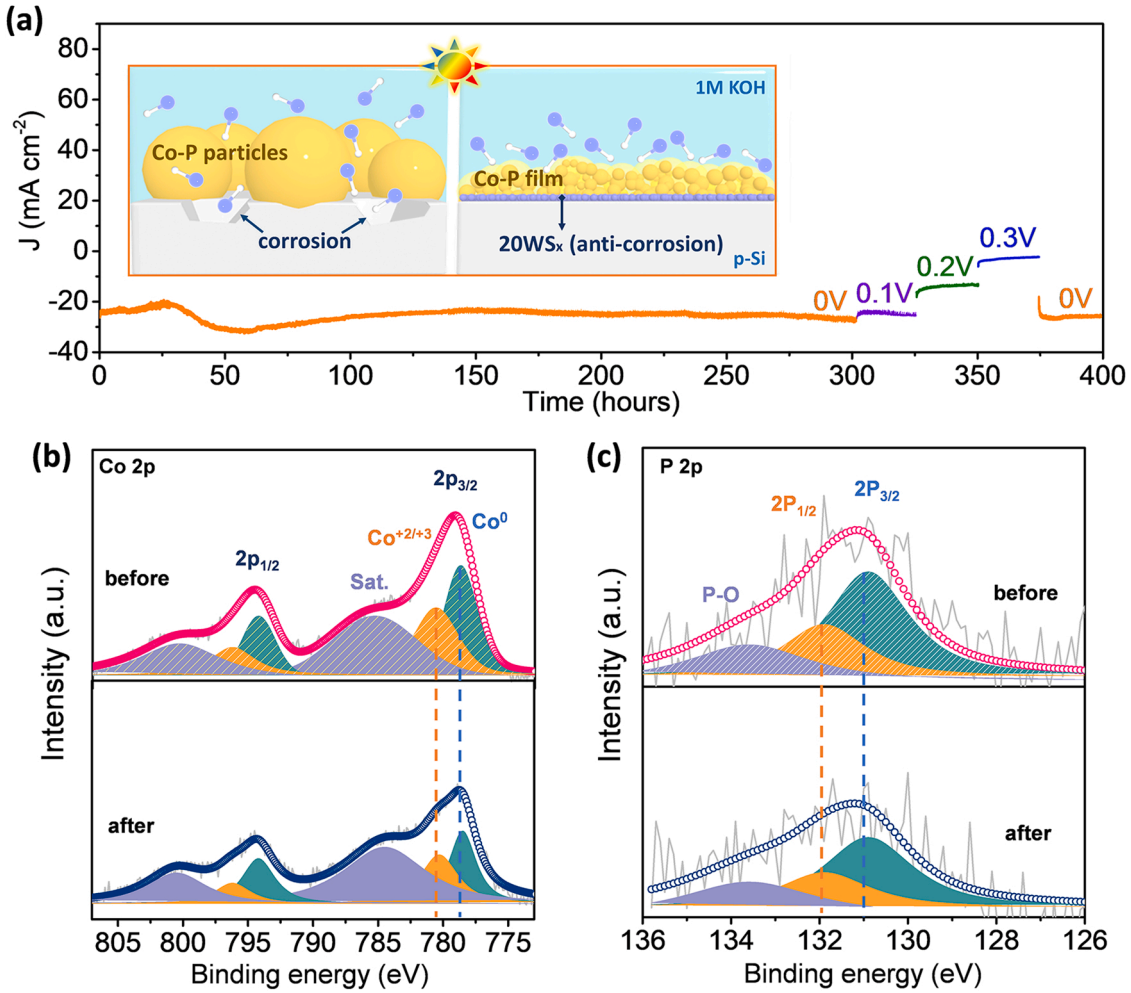

Fig. 4. (a) The chronoamperometric current–time profiles of Co-P/20WS_x/Si at 0, 0.1, 0.2, and 0.3 V_{RHE} in 1.0 M KOH. Schematic diagram of the anti-corrosive mechanism of Co-P/20WS_x/Si compared to Co-P/Si without 20WS_x protection layer inset. High-resolution XPS spectra of Co-P/20WS_x/Si in the regions of (b) Co 2p and (c) P 2p before and after the PEC-HER test.

3.4. Long-term stability testing

In order to determine the long-term stability of the as-prepared photocathodes, the chronoamperometric test at 0 V_{RHE} was conducted, as depicted in Fig. S8. After a duration time of 13 h, the decay of photocurrent density (calculated after 2-h activation) is in the following order: Co-P/Si (− 22%) > Co-P/5WS_x/Si (− 9%) > Co-P/30WS_x/Si (− 7%) > Co-P/20WS_x/Si (− 2%). The PEC long-term stability of the optimal Co-P/20WS_x/Si photocathode was confirmed in Fig. 4a. The Co-P/20WS_x/Si photocathode exhibits a photocurrent density of about − 27.5 mA cm^{-2} at an applied potential at 0 V_{RHE} over 300 h, which is better than other representative Si-based photocathodes in alkaline solutions so far in Table S2. After the 300-h duration test at 0 V_{RHE}, the potential is changed to + 0.1, + 0.2, and + 0.3 V_{RHE}, retaining the photocurrent densities of − 24.3, − 13.7, and − 2.5 mA cm^{-2}, respectively. Even if the applied potential is recovered to 0 V_{RHE} after 375 h, the Co-P/20WS_x/Si photocathode can still return to a stable photocurrent density of approximately − 28.4 mA cm^{-2}, and there is no noticeable fading of photocurrent density over 25 h, implying the excellent long-term durability. In addition, the LSV curves of Co-P/20WS_x/Si photocathode were collected before and after the stability test of 400 h in Fig. S9. It is found that the photocurrent density at 0 V_{RHE} increased slightly, which may be caused by the shedding of partial Co-P cocatalyst due to the violent hydrogen bubble popping, the remaining WS_x layer can prevent serious deep corrosion, as shown in the TEM image (Fig. S10). Notably, there is almost no negative shift in onset potential, demonstrating the superior adhesion of the interface of cocatalyst/protector/semiconductor. Moreover, the amount of evolved H_2 has a linear relationship with the illumination time, and a high Faradaic efficiency of near 99% is obtained (Fig. S11), revealing the full utilization of the photoexcited electrons for PEC HER.

The schematic diagram (the inset of Fig. 4a) shows the difference between the presence and absence of a uniform WS_x thin film as a protective layer on the stability against alkali corrosion and the morphology of the Co-P cocatalysts. The absence of WS_x thin film makes the Si lose effective resistance to alkali corrosion and results in the Co-P particle morphology, where the gaps between Co-P particles allow the alkaline electrolyte to immerse and corrode the unprotected Si. On the contrary, uniform 20WS_x thin film has good alkali corrosion resistance and could also be used as a nucleation substrate to form a dense and uniform Co-P film cocatalyst, confirming the superior long-term stability of Co-P/20WS_x/Si photocathode in 1.0 M KOH.

XPS measurements before and after the PEC-HER test within Co-P/20WS_x/Si photocathode were carried out to investigate the chemical change of the Co-P film cocatalyst. The signals of Co, P, C, and O elements were detected as displayed in the XPS survey spectrum (Fig. S12). In Co 2p XPS spectrum of the Co-P/20WS_x/Si photocathode (the top of Fig. 4b) before the long-term test, two dominant peaks at 778.7 (Co $2p_{3/2}$) and 794.2 eV (Co $2p_{1/2}$) are ascribed to Co^0, while the peak at around 780.6 eV (Co $2p_{3/2}$) and 796.3 eV (Co $2p_{1/2}$) are associated with $Co^{+2/+3}$ species, matching well with the Co-P alloy system [37,41,42]. The remaining peaks located at ~ 785.4 and 800.3 eV are satellite peaks. Moreover, the P 2p peaks (the top of Fig. 4c) could be deconvoluted into two doublets of P $2p_{3/2}$ (130.9 eV) and P $2p_{1/2}$ (131.9 eV), and a peak centered at 133.6 eV attributed to P–O species, possibly resulting from either the unavoidable oxidation of surface exposed to the air or remains from the electrochemical decomposition of NaH_2PO_2 [43]. It can also be demonstrated by the XPS spectrum of O 1s, which can be deconvoluted into two peaks of Co–O (530.8 eV) and P–O (531.9 eV) (Fig. S13). After the stability test in the alkaline electrolyte (the bottom of Fig. 4b–c), the XPS intensities of both Co 2p and P 2p peaks are reduced to a certain extent, which is responsible for the slightly higher photocurrent density observed in the LSV curve of Co-P/20WS_x/Si photocathode after the test. Except for this change, there is no noticeable peak shift for Co and P elements compared with fresh samples. Similarly, for the XRD pattern of the Co-P/20WSx/Si photocathode after the durability test, there is no peak change for the Co-P signal at 44.4°, as shown in Fig. S14. Therefore, the above results indicate that the Co-P cocatalyst within the optimized Co-P/20WS_x/Si photocathode is stable under such an alkaline environment, verifying the long-term durability of PEC HER.

4. Conclusion

The synergetic coupling of the Co-P film cocatalyst with the thin-film WSx protection layer on planar p-Si photocathode was investigated for efficient and durable PEC HER in alkaline solution. The thin-film WS_x protection layer plays a trifunctional role in 1) supporting excellent anti-corrosion for the Si substrate, 2) providing an appropriate nucleation base for the morphology optimization of Co-P cocatalyst with anti-reflection, and 3) promoting the electron transfer from photocathode to electrolyte. The Co-P cocatalyst could be modulated by controlling thin-film WS_x morphology to have the least light-blocking effect but retain the catalytic activity. The complementary integration of the Co-P film cocatalyst on WS_x/Si photocathode exhibits superior catalytic properties (an onset potential of + 0.47 V_{RHE}, a photocurrent density of − 25.1 mA cm^{-2} at 0 V_{RHE}), which benefits from the significantly enhanced reaction kinetics by promoting electron transfer. Meanwhile, through such rational structure, the optimal Co-P/WS_x/Si photocathode shows a long-term stability of 300 h at a high photocurrent density above − 25 mA cm^{-2} at 0 V_{RHE} without noticeable degradation in alkaline solution. This study provides a scalable strategy for future Si-based water splitting systems.

CRediT authorship contribution statement

Sijie Li: Conceptualization, Methodology, Investigation, Data curation, Writing – original draft. **Huiwen Lin**: Conceptualization, Methodology, Writing – review & editing. **Gaoliang Yang**: Conceptualization, Methodology. **Xiaohui Ren**: Formal analysis. **Shunqin Luo**: Visualization. **Xu-sheng Wang**: Validation, Resources. **Zhi Chang**: Software. **Jinhua Ye**: Conceptualization, Writing – review & editing, Supervision, Validation, Project administration, Funding acquisition.

Declaration of Competing Interest

The authors declare that they have no known competing financial interests or personal relationships that could have appeared to influence the work reported in this paper.

Acknowledgements

This work was financially supported by the World Premier International Research Center Initiative (WPI Initiative) on Materials Nanoarchitectonics (MANA), MEXT (Japan), Photoexcitonix Project in Hokkaido University, National Natural Science Foundation of China (Grant no. 21633004), State Scholarship Fund by China Scholarship Council (CSC) (201906370032).

Appendix A. Supplementary material

Supplementary data associated with this article can be found in the online version at doi:10.1016/j.apcatb.2021.120954.

References

[1] W. Vijselaar, R.M. Tiggelaar, H. Gardeniers, J. Huskens, Efficient and stable silicon microwire photocathodes with a nickel silicide interlayer for operation in strongly alkaline solutions, ACS Energy Lett. 3 (2018) 1086–1092, https://doi.org/10.1021/acsenergylett.8b00267.

[2] R. Fan, J. Zhou, W. Xun, S. Cheng, S. Vanka, T. Cai, S. Ju, Z. Mi, M. Shen, Highly efficient and stable Si photocathode with hierarchical MoS_2/Ni_3S_2 catalyst for solar

hydrogen production in alkaline media, Nano Energy 71 (2020), 104631, https://doi.org/10.1016/j.nanoen.2020.104631.
[3] X. Zhao, X. Li, D. Xiao, M. Gong, L. An, P. Gao, J. Yang, D. Wang, Isolated Pd atom anchoring endows cobalt diselenides with regulated water-reduction kinetics for alkaline hydrogen evolution, Appl. Catal. B Environ. 295 (2021), 120280, https://doi.org/10.1016/j.apcatb.2021.120280.
[4] Y. Men, Y. Tan, P. Li, X. Cao, S. Jia, J. Wang, S. Chen, W. Luo, Tailoring the 3d-orbital electron filling degree of metal center to boost alkaline hydrogen evolution electrocatalysis, Appl. Catal. B Environ. 284 (2021), 119718, https://doi.org/10.1016/j.apcatb.2020.119718.
[5] K. Sivula, R. van de Krol, Semiconducting materials for photoelectrochemical energy conversion, Nat. Rev. Mater. 1 (2016) 15010, https://doi.org/10.1038/natrevmats.2015.10.
[6] W. Zhou, F. Niu, S.S. Mao, S. Shen, Nickel complex engineered interface energetics for efficient photoelectrochemical hydrogen evolution over p-Si, Appl. Catal. B Environ. 220 (2018) 362–366, https://doi.org/10.1016/j.apcatb.2017.08.065.
[7] S. Li, G. Yang, P. Ge, H. Lin, Q. Wang, X. Ren, S. Luo, D. Philo, K. Chang, J. Ye, Engineering heterogeneous NiS_2/NiS cocatalysts with progressive electron transfer from planar p-Si photocathodes for solar hydrogen evolution, Small Methods 5 (2021), 2001018, https://doi.org/10.1002/smtd.202001018.
[8] C.-J. Chen, V. Veeramani, Y.-H. Wu, A. Jena, L.-C. Yin, H. Chang, S.-F. Hu, R.-S. Liu, Phosphorous-doped molybdenum disulfide anchored on silicon as an efficient catalyst for photoelectrochemical hydrogen generation, Appl. Catal. B Environ. 263 (2020), 118259, https://doi.org/10.1016/j.apcatb.2019.118259.
[9] M.G. Kast, L.J. Enman, N.J. Gurnon, A. Nadarajah, S.W. Boettcher, Solution-deposited F:SnO_2/TiO_2 as a base-stable protective layer and antireflective coating for microtextured buried-junction H_2-evolving Si photocathodes, ACS Appl. Mater. Interfaces 6 (2014) 22830–22837, https://doi.org/10.1021/am506999p.
[10] J. Zheng, Y. Lyu, R. Wang, C. Xie, H. Zhou, S.P. Jiang, S. Wang, Crystalline TiO_2 protective layer with graded oxygen defects for efficient and stable silicon-based photocathode, Nat. Commun. 9 (2018) 3572, https://doi.org/10.1038/s41467-018-05580-z.
[11] S. Hu, M.R. Shaner, J.A. Beardslee, M. Lichterman, B.S. Brunschwig, N.S. Lewis, Amorphous TiO_2 coatings stabilize Si, GaAs, and GaP photoanodes for efficient water oxidation, Science 344 (2014) 1005, https://doi.org/10.1126/science.1251428.
[12] Y.W. Chen, J.D. Prange, S. Dühnen, Y. Park, M. Gunji, C.E.D. Chidsey, P. C. McIntyre, Atomic layer-deposited tunnel oxide stabilizes silicon photoanodes for water oxidation, Nat. Mater. 10 (2011) 539–544, https://doi.org/10.1038/nmat3047.
[13] H. Lin, S. Li, G. Yang, K. Zhang, D. Tang, Y. Su, Y. Li, S. Luo, K. Chang, J. Ye, In situ assembly of MoS_x thin-film through self-reduction on p-Si for drastic enhancement of photoelectrochemical hydrogen evolution, Adv. Funct. Mater. 31 (2021), 2007071, https://doi.org/10.1002/adfm.202007071.
[14] Y. Zhong, Y. Shao, F. Ma, Y. Wu, B. Huang, X. Hao, Band-gap-matched CdSe QD/WS_2 nanosheet composite: size-controlled photocatalyst for high-efficiency water splitting, Nano Energy 31 (2017) 84–89, https://doi.org/10.1016/j.nanoen.2016.11.011.
[15] Y. Yang, H. Fei, G. Ruan, Y. Li, J.M. Tour, Vertically aligned WS_2 nanosheets for water splitting, Adv. Funct. Mater. 25 (2015) 6199–6204, https://doi.org/10.1002/adfm.201502479.
[16] Y. Shi, B. Zhang, Recent advances in transition metal phosphide nanomaterials: synthesis and applications in hydrogen evolution reaction, Chem. Soc. Rev. 45 (2016) 1529–1541, https://doi.org/10.1039/c5cs00434a.
[17] N. Jiang, B. You, M. Sheng, Y. Sun, Electrodeposited cobalt-phosphorous-derived films as competent bifunctional catalysts for overall water splitting, Angew. Chem. Int. Ed. 54 (2015) 6251–6254, https://doi.org/10.1002/anie.201501616.
[18] J.H. Kim, S. Han, Y.H. Jo, Y. Bak, J.S. Lee, A precious metal-free solar water splitting cell with a bifunctional cobalt phosphide electrocatalyst and doubly promoted bismuth vanadate photoanode, J. Mater. Chem. A 6 (2018) 1266–1274, https://doi.org/10.1039/C7TA09134F.
[19] A. Chunduri, S. Gupta, O. Bapat, A. Bhide, R. Fernandes, M.K. Patel, V. Bambole, A. Miotello, N. Patel, A unique amorphous cobalt-phosphide-boride bifunctional electrocatalyst for enhanced alkaline water-splitting, Appl. Catal. B Environ. 259 (2019), 118051, https://doi.org/10.1016/j.apcatb.2019.118051.
[20] K. Xu, H. Cheng, H. Lv, J. Wang, L. Liu, S. Liu, X. Wu, W. Chu, C. Wu, Y. Xie, Controllable surface reorganization engineering on cobalt phosphide nanowire arrays for efficient alkaline hydrogen evolution reaction, Adv. Mater. 30 (2018), 1703322, https://doi.org/10.1002/adma.201703322.
[21] Y. Li, H. Li, K. Cao, T. Jin, X. Wang, H. Sun, J. Ning, Y. Wang, L. Jiao, Electrospun three dimensional Co/CoP@nitrogen-doped carbon nanofibers network for efficient hydrogen evolution, Energy Storage Mater. 12 (2018) 44–53, https://doi.org/10.1016/j.ensm.2017.11.006.
[22] L.-A. Stern, L. Liardet, M.T. Mayer, C.G. Morales-Guio, M. Grätzel, X. Hu, Photoelectrochemical deposition of CoP on cuprous oxide photocathodes for solar hydrogen production, Electrochim. Acta 235 (2017) 311–316, https://doi.org/10.1016/j.electacta.2017.03.074.
[23] C.W. Roske, E.J. Popczun, B. Seger, C.G. Read, T. Pedersen, O. Hansen, P. C. Vesborg, B.S. Brunschwig, R.E. Schaak, I. Chorkendorff, H.B. Gray, N.S. Lewis, Comparison of the performance of CoP-coated and Pt-coated radial junction n^+p-silicon microwire-array photocathodes for the sunlight-driven reduction of water to H_2(g), J. Phys. Chem. Lett. 6 (2015) 1679–1683, https://doi.org/10.1021/acs.jpclett.5b00495.
[24] X.-Q. Bao, M. Fatima Cerqueira, P. Alpuim, L. Liu, Silicon nanowire arrays coupled with cobalt phosphide spheres as low-cost photocathodes for efficient solar hydrogen evolution, Chem. Commun. 51 (2015) 10742–10745, https://doi.org/10.1039/C5CC02331A.
[25] T.R. Hellstern, J.D. Benck, J. Kibsgaard, C. Hahn, T.F. Jaramillo, Engineering cobalt phosphide (CoP) thin film catalysts for enhanced hydrogen evolution activity on silicon photocathodes, Adv. Energy Mater. 6 (2016), 1501758, https://doi.org/10.1002/aenm.201501758.
[26] S.M. Thalluri, B. Wei, K. Welter, R. Thomas, V. Smirnov, L. Qiao, Z. Wang, F. Finger, L. Liu, Inverted pyramid textured p-silicon covered with Co_2P as an efficient and stable solar hydrogen evolution photocathode, ACS Energy Lett. 4 (2019) 1755–1762, https://doi.org/10.1021/acsenergylett.9b00964.
[27] S.M. Thalluri, J. Borme, K. Yu, J. Xu, I. Amorim, J. Gaspar, L. Qiao, P. Ferreira, P. Alpuim, L. Liu, Conformal and continuous deposition of bifunctional cobalt phosphide layers on p-silicon nanowire arrays for improved solar hydrogen evolution, Nano Res. 11 (2018) 4823–4835, https://doi.org/10.1007/s12274-018-2070-4.
[28] I. Paseka, J. Velicka, Hydrogen evolution and hydrogen sorption on amorphous smooth Me-P(x) (Me = Ni, Co and Fe-Ni) electrodes, Electrochim. Acta 42 (1997) 237–242, https://doi.org/10.1016/0013-4686(96)00149-1.
[29] H. Liu, X. Ma, H. Hu, Y. Pan, W. Zhao, J. Liu, X. Zhao, J. Wang, Z. Yang, Q. Zhao, H. Ning, M. Wu, Robust NiCoP/CoP heterostructures for highly efficient hydrogen evolution electrocatalysis in alkaline solution, ACS Appl. Mater. Interfaces 11 (2019) 15528–15536, https://doi.org/10.1021/acsami.9b00592.
[30] C.D. Nguyen, T.L.M. Pham, T.Y. Vu, V.B. Mai, K.L. Vu-Huynh, Hierarchical Zn-Co-P nanoneedle arrays supported on three-dimensional framework as efficient electrocatalysts for hydrogen evolution reaction in alkaline condition, J. Electroanal. Chem. 858 (2020), https://doi.org/10.1016/j.jelechem.2019.113803.
[31] M. Cabán-Acevedo, M.L. Stone, J.R. Schmidt, J.G. Thomas, Q. Ding, H.-C. Chang, M.-L. Tsai, J.-H. He, S. Jin, Efficient hydrogen evolution catalysis using ternary pyrite-type cobalt phosphosulphide, Nat. Mater. 14 (2015) 1245–1251, https://doi.org/10.1038/nmat4410.
[32] N. Bai, Q. Li, D. Mao, D. Li, H. Dong, One-step electrodeposition of Co/CoP film on Ni foam for efficient hydrogen evolution in alkaline solution, ACS Appl. Mater. Interfaces 8 (2016) 29400–29407, https://doi.org/10.1021/acsami.6b07785.
[33] S. Li, P. Ge, F. Jiang, H. Shuai, W. Xu, Y. Jiang, Y. Zhang, J. Hu, H. Hou, X. Ji, The advance of nickel-cobalt-sulfide as ultra-fast/high sodium storage materials: the influences of morphology structure, phase evolution and interface property, Energy Storage Mater. 16 (2019) 267–280, https://doi.org/10.1016/j.ensm.2018.06.006.
[34] S. Liu, Y. Xu, D. Chanda, L. Tan, R. Xing, X. Li, L. Mao, N. Kazuya, A. Fujishima, Ultrathin WS_2 nanosheets vertically aligned on TiO_2 nanobelts as efficient alkaline hydrogen evolution electrocatalyst, Int. J. Hydrog. Energy 45 (2020) 1697–1705, https://doi.org/10.1016/j.ijhydene.2019.11.018.
[35] V. Ezhilselvi, H. Seenivasan, P. Bera, C. Anandan, Characterization and corrosion behavior of Co and Co–P coatings electrodeposited from chloride bath, RSC Adv. 4 (2014) 46293–46304, https://doi.org/10.1039/C4RA08226E.
[36] V.E. Selvi, H. Seenivasan, K.S. Rajam, Electrochemical corrosion behavior of pulse and DC electrodeposited Co–P coatings, Surf. Coat. Technol. 206 (2012) 2199–2206, https://doi.org/10.1016/j.surfcoat.2011.09.063.
[37] P. Bera, H. Seenivasan, K.S. Rajam, V.K. William Grips, Characterization of amorphous Co–P alloy coatings electrodeposited with pulse current using gluconate bath, Appl. Surf. Sci. 258 (2012) 9544–9553, https://doi.org/10.1016/j.apsusc.2012.05.115.
[38] J. Zhao, L. Cai, H. Li, X. Shi, X. Zheng, Stabilizing silicon photocathodes by solution-deposited Ni–Fe layered double hydroxide for efficient hydrogen evolution in alkaline media, ACS Energy Lett. 2 (2017) 1939–1946, https://doi.org/10.1021/acsenergylett.7b00597.
[39] Q. Ding, F. Meng, C.R. English, M. Cabán-Acevedo, M.J. Shearer, D. Liang, A. S. Daniel, R.J. Hamers, S. Jin, Efficient photoelectrochemical hydrogen generation using heterostructures of Si and chemically exfoliated metallic MoS_2, J. Am. Chem. Soc. 136 (2014) 8504–8507, https://doi.org/10.1021/ja5025673.
[40] G. Yang, S. Li, X. Wang, B. Ding, Y. Li, H. Lin, D. Tang, X. Ren, Q. Wang, S. Luo, J. Ye, A universal strategy boosting photoelectrochemical water oxidation by utilizing MXene nanosheets as hole transfer mediators, Appl. Catal. B Environ. 297 (2021), 120268, https://doi.org/10.1016/j.apcatb.2021.120268.
[41] K. Liu, C. Zhang, Y. Sun, G. Zhang, X. Shen, F. Zou, H. Zhang, Z. Wu, E.C. Wegener, C.J. Taubert, J.T. Miller, Z. Peng, Y. Zhu, High-performance transition metal phosphide alloy catalyst for oxygen evolution reaction, ACS Nano 12 (2018) 158–167, https://doi.org/10.1021/acsnano.7b04646.
[42] W. Zhen, Y. Guo, Y. Wu, G. Lu, Co–P/graphene alloy catalysts doped with Cu and Ni for efficient photocatalytic hydrogen generation, New J. Chem. 41 (2017) 13804–13811, https://doi.org/10.1039/C7NJ01598D.
[43] Y. Zhang, L. Gao, E.J.M. Hensen, J.P. Hofmann, Evaluating the stability of Co_2P electrocatalysts in the hydrogen evolution reaction for both acidic and alkaline electrolytes, ACS Energy Lett. 3 (2018) 1360–1365, https://doi.org/10.1021/acsenergylett.8b00514.